A recurrent missense variant in ITPR3 causes demyelinating Charcot-Marie-Tooth with variable severity

Danique Beijer,[1,2,†] Maike F. Dohrn,[1,3,†] Adriana Rebelo,[1] Matt C. Danzi,[1] Bianca Rose Grosz,[4] Melina Ellis,[4] Kishore R. Kumar,[5] Steve Vucic,[6] Horia Vais,[7] Jillian S. Weissenrieder,[7] Olesia Lunko,[7] Usha Paudel,[7] Leah C. Simpson,[7] Jacquelyn Raposo,[1] Mario Saporta,[1,8] Yeisha Arcia,[1] Isaac Xu,[1] Shawna Feely,[9] Christopher J. Record,[10] Julian Blake,[10,11] Mary M. Reilly,[10] Steven Scherer,[12] Marina Kennerson,[4,5] Yi-Chung Lee,[13] J. Kevin Foskett,[7,14] Michael Shy,[15] Inherited Neuropathy Consortium and Stephan Zuchner[1]

[†]**These authors contributed equally to this work.**

Abstract

Charcot-Marie-Tooth (CMT) disease is a neuromuscular disorder affecting the peripheral nervous system. The diagnostic yield in demyelinating CMT (CMT1) is typically ~80-95%, of which at least 60% is due to the *PMP22* gene duplication. The remainder of CMT1 is more genetically heterogeneous.

We used whole exome and whole genome sequencing data included in the GENESIS database to investigate novel causal genes and mutations in a cohort of ~2,670 individuals with CMT neuropathy.

A recurrent heterozygous missense variant p.Thr1424Met in the recently described CMT gene *ITPR3*, encoding IP_3R3 (inositol 1,4,5-trisphosphate receptor 3) was identified. This previously reported p.Thr1424Met change was present in 33 affected individuals from nine unrelated families from multiple populations, representing an unusual recurrence rate at a mutational hotspot, strengthening the gene-disease relationship (GnomADv4 allele frequency 1.76e-6). Sanger sequencing confirmed the co-segregation of the CMT phenotype with the presence of the mutation in autosomal dominant and *de novo* inheritance patterns, including a four-generation family with multiple affected second-degree cousins.

Probands from all families presented with slow nerve conduction velocities, matching the diagnostic category of CMT1. Remarkably, we observed a uniquely variable clinical phenotype for age at onset and phenotype severity in p.Thr1424Met carrying patients, even within families. Finally, we present data supportive of a dominant-negative effect of the p.Thr1424Met mutation with associated changes in protein expression in patient-derived cells.

Author affiliations:

1 Department of Human Genetics and John P. Hussman Institute for Human Genomics, University of Miami Miller School of Medicine, Miami, 33136 FL, USA

2 Translational Genomics of Neurodegenerative Diseases, Hertie-Institute for Clinical Brain Research, University of Tübingen, 72076 Tübingen, Germany

3 Department of Neurology, Medical Faculty RWTH Aachen University, 52074 Aachen, Germany

4 Northcott Neuroscience Laboratory ANZAC Research Institute, Sydney Local Health District, School of Medical Sciences, University of Sydney, NSW 2139, Sydney, Australia

5Department of Neurology and Molecular Medicine Laboratory, Sydney Medical School, University of Sydney, Concord Hospital, NSW 2139, Sydney, Australia

6 Brain and Nerve Research Centre, Concord Hospital, Sydney Medical School, University of Sydney, NSW 2139, Sydney, Australia

7 Department of Physiology, Perelman School of Medicine, University of Pennsylvania, Philadelphia, 19104 PA, USA

8 Department of Neurology, University of Miami Miller School of Medicine, Miami, 33136 FL, USA

9 Neurology, The University of Iowa Roy J and Lucille A Carver College of Medicine, Iowa City, 55242 IA, USA

10 Centre for Neuromuscular Diseases, UCL Queen Square Institute of Neurology, Queen Square, WC1N36BG London, United Kingdom

11 Department of Clinical Neurophysiology, Norfolk and Norwich University Hospital, NR4 7UY Norwich, UK

12 Department of Neurology, The Perelman School of Medicine, University of Pennsylvania, Philadelphia, 19104 PA, USA

13 Department of Neurology, Taipei Veterans General Hospital, 112 Taipei, Taiwan

14 Department of Cell and Developmental Biology, Perelman School of Medicine, University of Pennsylvania, Philadelphia, 19104 PA, USA

15 Department of Neurology, University of Iowa, Carver College of Medicine, Iowa City, 55242 IA, USA

Correspondence to: Stephan Züchner

University of Miami Miller School of Medicine

Biomedical Research Building (BRB)

Room 616, LC: M-860

1501 NW 10th Avenue

Miami, FL 33136, USA

E-mail: szuchner@med.miami.edu

Running title: ITPR3 causes remarkably variable CMT1

Keywords: demyelinating Charcot-Marie-Tooth disease; next-generation sequencing; inositol 1,4,5-trisphosphate

Abbreviations: CMT – Charcot Marie-Tooth disease; CMT1 – demyelinating Charcot Marie-Tooth disease; CMT examination score - CMTES; ER - endoplasmic reticulum; next-generation sequencing – NGS; WES - whole exome sequencing; WGS - whole genome sequencing

Introduction

The modulation of cytoplasmic Ca^{2+} concentrations is a ubiquitous cellular process that regulates numerous important cellular pathways.[1] Inositol 1,4,5-trisphosphate receptors (IP_3R), located in the endoplasmic reticulum (ER), are capable of releasing internal Ca^{2+} stores and play an essential role in this process. Humans have three IP_3R subtypes (IP_3R1, IP_3R2, and IP_3R3), encoded by three separate genes *ITPR1*, *ITPR2*, and *ITPR3*.[1-3]

All three IP_3Rs assemble into tetrameric channel complexes composed of either identical (homotetramer) or different IP_3R subtypes (heterotetramer). IP_3 binds to the IP_3R within the complex promoting subsequent release of Ca^{2+} from the ER. While overlapping in their general function and structure, the three different IP_3R subtypes are different in their amino acid sequence as well as their IP_3 affinity and modulation by Ca^{2+} and ATP.[3-6] Furthermore, the different isoforms seem distinctly expressed in a spatiotemporal manner, with different combinations of subtypes co-expressed in tissues and developmental stages. Subcellular differences in subtype localization are also thought to modulate Ca^{2+} release pattern and downstream functional outcomes.[6]

The differences in cellular, and potentially subcellular, localization appear distinctly linked with different human diseases. IP_3R1, encoded by *ITPR1*, is highly expressed in Purkinje cells and, when mutated, causes cerebellar ataxia in both mice and humans.[7,8] IP_3R3 is predominantly expressed in the paranodal region in Schwann cells.[9] In a limited number of families, mutations in *ITPR3* have been linked with the peripheral nervous system disorder Charcot-Marie-Tooth disease.[10-12]

Charcot-Marie-Tooth (CMT) disease is a rare neuromuscular disorder affecting the peripheral nervous system. The diagnostic yield in demyelinating CMT (CMT1) is typically ~80-95%, of which at least 60% is due to the *PMP22* gene duplication.[13] The remainder of CMT1 is more genetically heterogeneous.

In this study, we present a highly recurrent *ITPR3* (NM_002224.4) c.4271C>T p.Thr1424Met missense variant in exon 32 (hg38), first identified by Schabhuttl *et al.*[10] in nine families with demyelinating CMT that further confirms the association between *ITPR3* mutations and specifically demyelinating Charcot-Marie-Tooth disease. Our extended dataset comprising 33

affected individuals significantly strengthens the association between the *ITPR3* and CMT beyond the initially observed limited number of families. Functional assessment of the recurrent p.Thr1424Met mutation demonstrated protein loss in patient fibroblasts for IP_3R3. The recurrent nature of the mutation allowed us to perform an in-depth analysis of the clinical phenotype associated with the mutation, demonstrating a uniquely high phenotypic variability between individuals.

Materials and methods

Patient recruitment and selection

Patients with rare presumed genetic neuropathy phenotypes were recruited at neuropathy reference centers worldwide. Informed consent for study participation was obtained based on the local and legal guidelines. Our study complies with the Declaration of Helsinki. For inclusion in the study, patients were considered genetically undiagnosed, meaning at the time of examination, no known genetic cause was known for the patient.

Clinical examination and data collection

All patients were examined by experienced neurologists, and relevant information was collected using a standardized clinical record form (Table 1, Supplementary table 1 and Supplementary table 2). Cohort characteristics were determined by calculating means and counts, without additional statistical testing (Table 1).

Next-generation sequencing

Whole exome sequencing (WES) or whole genome sequencing (WGS) was performed on at least the proband for each family. For WES, exome enrichment was performed using the SureSelect Human All Exon Kit (Agilent, Santa Clara, CA, USA) with subsequent sequencing for both WES and WGS on a HiSeq 2500 instrument (Illumina, San Diego, CA, USA). The Burrows-Wheeler aligner was used for sequence alignment and Freebayes for variant calling. WES and

WGS data were uploaded into the GENESIS platform, which was also used to analyze potential pathogenic variants.[14] Segregation of candidate variants was subsequently assessed by Sanger sequencing in all available family members.

Cell culture

Fibroblast cells were cultured from skin biopsies from the proband of family 1, and unrelated healthy control individuals. Fibroblast, HEK293 and rat Schwannoma cells (RT4-D6P2T; ATCC, Manassas, VA) were cultured in Dulbecco's modified Eagle medium containing 10% (v/v) fetal bovine serum (FBS), 1% (v/v) 100x antibiotics (penicillin and streptomycin) and 1% (v/v) 100mM sodium pyruvate under humidified air at 37°C in 5% CO_2. U2OS cells were cultured in McCoy medium with 10% (v/v) FBS, 1% (v/v) 100x antibiotics and 1% (v/v) 100mM sodium pyruvate. Healthy control iPSC-derived motor neurons were generated and cultured according to a previously established protocol and used for protein analysis.[15]

Over-expression model

Two vectors containing the wild-type (WT) human *ITPR3* [NM_002224.3] ORF under a CMV promoter, one with C-terminal MYC and one with C-terminal 3xHA tag were obtained from GeneCopoeia [Y5263]. Site-directed mutagenesis to introduce the p.Thr1424Met mutation was performed using the Q5 site-directed mutagenesis kit (NEB), implementation of the mutation was confirmed by Sanger sequencing. HEK293 cells were transfected with either the WT or p.Thr1424Met mutant plasmid using Lipofectamine 3000 (Invitrogen). Cells were collected 24 hours post transfection.

Western blot

Cells for western blot were lysed with RIPA buffer containing protease inhibitors (cOmplete™ Protease Inhibitor Cocktail, Roche) and protein concentrations were measured with a BCA kit (Pierce™ BCA Protein Assay, ThermoScientific). Protein lysates were combined with 4x sample buffer with SDS and size fractioned on a 4-12% SDS-PAGE gels (NuPAGE™ 4 to 12%, Bis-

Tris, Invitrogen). Proteins were transferred to PVDF membranes which were then blocked with 5% (w/v) milk in TBST (10mM Tris.HCl, 15mM NaCl, 0.05% Tween 20 at pH 7.5). The following dilutions of primary antibodies were incubated for 2 h at room temperature or overnight at 4ºC: rabbit IP_3R1 1:400 (Yule lab), mouse IP_3R2 1:1000 (Santa Cruz: sc-398434), mouse IP_3R3 1:2000 (BD Biosciences: 2/IP3R-3), mouse GAPDH 1:1000 (Santa Cruz: sc-32233), mouse HA (1:1000, 6E2 Cell Signaling), mouse MYC (1:1000, 9B11 Cell Signaling), and beta-tubulin (1:2000, D-10 Santa Cruz, sc-5274). An appropriate dilution of secondary antibodies (1:4000) were incubated for 1 h at room temperature: anti-mouse HRP (7076 Cell Signaling), anti-rabbit HRP (7074 Cell Signaling).

Co-immunoprecipitation

HEK cells were seeded in 10cm dishes and at 70% confluency were co-transfected in the following construct combinations: (1) ITPR3-WT-HA and ITPR3-WT-MYC, (2) ITPR3-WT-HA and ITPR3-Thr1424Met-MYC, (3) ITPR3-Thr1424Met-HA and ITPR3-Thr1424Met-MYC, using Lipofectamine 3000 (Invitrogen). Cells were harvested 24 hours post transfection and lysed using IP buffer (Pierce™ IP Lysis Buffer, Thermo Scientific, 87787). Co-immunoprecipitation was performed using Dynabeads™ Protein G (Invitrogen, 10009D) coated with mouse HA antibody (1:200, C29F4 Cell Signaling), with subsequent immunoblotting for mouse HA (1:1000, 6E2 Cell Signaling) or mouse MYC (1:1000, 9B11 Cell Signaling) (Supplementary 2B left and right) and mouse GAPDH 1:1000 (sc-32233, Santa Cruz) or rabbit GAPDH 1:1000 (14C10, Cells signaling). Appropriate secondary antibodies were used 1:4000 for 1h at room temperature: anti-mouse HRP (7076 Cell Signaling), anti-rabbit HRP (7074 Cell Signaling).

RNA sequencing analysis

Re-analysis of transcriptomics data from Peng *et al.* [16] was performed using the iDEP.95 software to normalize the data and obtain CPM values.[16,17]

RNA analysis of patient fibroblasts

Fibroblasts for RNA analysis were seeded in triplicate and stimulated with cycloheximide as previously described.[18] Fibroblasts for RNA extraction were subsequently collected and washed with PBS, before freezing at -80ºC. RNA extraction was performed using the Qiagen RNeasy Mini Plus kit and reverse transcribed template prepared using the QuantiTect Reverse Transcription kit (Qiagen). Primers were designed to amplify cDNA of *ITPR3* exons 31-34 (Forward: 5'-CAGCCCCCTCATGTACCACA-3' , Reverse: 5'-GCTGTAGCCACGGACACTCG-3') and Sanger sequenced.

Immunostaining

U2OS cells were seeded in 8-well slides (µ-Slide 8 Well slides, Ibidi) at 70% confluency, and left to attach overnight. Cells were then co-transfected using Lipofectamine™3000 (Invitrogen) with ITPR3-WT-HA and either *ITPR3*-WT-MYC or *ITPR3*-Thr1424Met-MYC. The transfected cells were subsequently probed with rabbit MYC (1:100, 9B11 Cell Signaling) and mouse HA (1:100, 6E2 Cell Signaling) antibodies for 2h at room temperature, secondary antibodies mouse-594, rabbit-488 (1:400) for 1h at room temperature and DAPI (1:1000).

Single IP_3R3 channel electrophysiology

HEK293T cells were cultured in 15 cm plates using L-glutamine, 4.5g/L glucose and 1% sodium pyruvate DMEM medium (Corning cat. # MT10-013-CM), supplemented with 10% FBS (HyClone), 1% antibiotic-antimycotic (gibco, 15240-062), at 37°C in 5% CO_2. Medium was refreshed every 2-3 days. HEK293T cells with all three IP_3R isoforms deleted (Kerafast, EUR030) were transfected with 50 µg of pIRES-ITPR3-WT-GFP or pIRES-ITPR3-T1424M-GFP plasmids for 48h with Lipofectamine 3000 (ThermoFisher Scientific, L3000001). Briefly, 87 µL of Lipofectamine 3000 reagent was mixed into 1000 µL OptiMEM (ThermoFisher Scientific, 31985070) for Mix 1, and 112 µL of P3000 and 50 µg plasmid were mixed into 1000 µL OptiMEM for Mix 2. 1000 µL of Mix 1 was added to Mix 2 by inversion, then allowed to sit for 10 min at room temperature before being added dropwise to >80% confluent 15 cm plates in

complete media. Cells were then incubated at 5% CO_2 and 37°C for 48 h before electrophysiology studies. Patch-clamp electrophysiology of nuclei isolated from transiently transfected HEK293T cells was performed as described [19].The bath and pipette solutions contained (in mM): 140 KCl and 10 HEPES (pH 7.3). The bath solution contained 0.06 mM $CaCl_2$ and 0.5 BAPTA (free $[Ca^{2+}] < 70$ nM calculated with MaxChelator). Pipette solutions facing the cytoplasmic side of the IP_3R3 contained either 2 μM or 30 μM free $[Ca^{2+}]$ ($[Ca^{2+}]_{free}$) buffered with either 0.5 mM 5,50-dibromo 1,2-bis(o-aminophenoxy)ethane-N,N,N0,N0-tetraacetic acid (diBrBAPTA, Invitrogen D-1211 or Santa Cruz Biotechnology sc-2273516) or 0.5 mM NTA (nitrilotriacetic acid; Sigma). Pipette solutions also contained 0.5 mM Na_2ATP and either sub-saturating 1 μM or saturating 10 μM IP_3 (Santa Cruz Biotechnology sc-201521) to stimulate IP_3R3 channel gating [20,21]. IP_3R3 channel-current traces under constant applied potential (V_{app}) were acquired at room temperature as described, digitized at 5 kHz, and anti-aliasing filtered at 1 kHz. All V_{app} were relative to the reference bath electrode [22]. IP_3R3 channel gating characteristics—number of active channels observed (NA) and open probability (P_o)—were derived from current traces using semi-automatic QuB [23] and fully-automatic [24] software and manually using IGOR Pro software (Wavemetrics). Only current traces long enough for NA to be determined with >99% confidence were used for statistical analysis [25].

Results

Genetic findings

In the analysis of >2,670 next-generation sequencing (NGS) datasets of patients with peripheral neuropathies and 16,000 controls (non-neuropathy phenotypes), we discovered the presence of a recurrent missense mutation in *ITPR3,* a gene previously associated with CMT in a limited number of families. [10,11] After the initial identification of the *ITPR3* p.Thr1424Met (NM_002224.4: c.4271C>T, p.Thr1424Met) variant in NGS data of 9 families, additional segregation analyses by Sanger sequencing allowed assessment of the variant in a total of 72 individuals, in which 33 were affected and 39 were unaffected. Co-segregation of the p.Thr1424Met variant and the neuropathy phenotype confirmed a dominant inheritance pattern in six of the families and *de novo* inheritance in one family (Figure 1). Family 1 had 12 affected

individuals available for our study, which supported a two-point LOD score of 3.6 for this variant. The p.Thr1424Met variant has a CADD score of 34, a dominant MAVERICK score of 0.90, AlphaMissense score of 0.9495, one occurrence in 566,682 chromosomes in GnomAD v4, and a missense constraint Z score of 5.26.[26-28]

The recurrence of the p.Thr1424Met change in nine families is likely due to a mutational hot spot. The genetic backgrounds and ethnicities include European, Taiwanese, and Sri Lankan origin (Supplementary table 1). Further, family 5 was a *de novo* case with confirmed paternity (Figure 1). We investigated this possibility of a major haplotype by establishing a SNV pattern in family 1, based on WGS in five individuals [1.III.03, 1.III.1, 1.IV.06, 1.IV.10 and 1.V.05] and assessing whether this SNV pattern was found in the other families. We found no evidence for a founder effect in any of the families, supporting the likelihood of a mutational hot spot.

Clinical findings

Herein, we describe 33 individuals from nine unrelated families, all carrying the same heterozygous *ITPR3* mutation, co-segregating with the phenotype (Figure 1, Table 1, Supplementary Fig. 1, Supplementary Fig. 2). The mean age at examination was 44.2 years, ranging from 2 to 86 years. Fifteen of the examined individuals were male, and 18 were female. With an estimated mean age of onset of 21.3 years, walking difficulties were reported as the most common first and overall symptom (present in 72.4% of cases). At the time of examination, 71.4% of patients reported impaired upper limb fine motor skills, which were first noticed 11 years post onset (32.4 years). Four individuals reported neither walking difficulties nor impaired dexterity. Clinically, we observed from mild to severe, distally pronounced weakness and atrophies, combined with distal sensory deficits in all modalities (Figure 2A, 2B). CMTES scores were available in 22 individuals, providing a broad range from 0 to 25 points (mean 10 points) at examination (Table 1, Supplementary table 1).

Even in individuals previously considered clinically unaffected, nerve conduction velocity slowing was in the range from intermediate to demyelinating, 20m/s – 38m/s at ulnar nerves (Supplementary Table 2), with remarkable intrafamilial variability. When available, EMG showed length-dependent chronic neurogenic changes, partially accompanied by additional signs

of ongoing denervation such as fibrillations and positive sharp waves. Nerve ultrasound, performed in only one patient, showed partial, scattered rather than homogeneous thickening of the peripheral nerve cross sectional areas. Spinal MRI revealed pronounced signs of nerve root enlargement in three examined individuals.

Overall, our cohort presented with a specific clinical picture consisting of a length-dependent, sensorimotor, demyelinating or intermediate polyneuropathy with walking difficulties as the most common and typically first symptom. The repeatedly observed clinical variability of disease severity is a notable feature of p.Thr1424Met *ITPR3* neuropathy. Exemplary family descriptions are as follows:

1. With ten affected individuals available for genotype-phenotype correlations, the largest reported herein family is family 1. Following normal motor milestones and an unremarkable, active childhood, the now 46-year-old proband of family 1 (I.IV.06) reported first difficulties running and walking at the age of 13 years. She began to use insoles and AFOs and still tried to competitively run with them. From college age on, she regularly ambulated with crutches, and started to occasionally use a wheelchair at the age of 30 years. At the most recent examination (Figure 2A), she presented with a high-grade distally pronounced flaccid tetraparesis with significantly impaired fine motor skills, reduced core strength and hyperlordosis, as well as a soft voice due to limited breath support, due to suspected neuromuscular respiratory involvement. We found distal sensory deficits in all modalities in lower extremities. Deep tendon reflexes were abolished. Nerve conduction studies last performed at the age of 33 years revealed low and fragmented motor amplitudes (0.2 mV for the left median nerve) and significantly reduced conduction velocities (15.6m/s at the right ulnar and 26.9 m/s at the left median nerve). Her CMTES was 22 at 47 years of age, while her mother (1.III.03) presented a milder course, with maintained walking ability (using bilateral crutches) at the age of 76 years and a CMTES of 19 (Figure 2A). The mother's younger cousin, (1.III.11, 69 years), was wheelchair-bound with complete flaccid paralysis of distal arm and leg muscles, including wrist extensors, and an CMTES of 25 (Figure 2A). Comparatively, a male cousin (I.IV.10) of the proband displayed mild sensory deficits in distal lower legs and feet, mild weakness of toe extensors, and atrophies of lower calves and intrinsic foot muscles and has a CMTES of 4. He considered himself unaffected, however, his ten-year-old son had just been diagnosed with CMT with difficulties running and reduced

nerve conduction velocities (not shown). This large range of clinical impairment was a common observation in other families (Figure 2B).

2. A very early disease onset has been observed in family 3, with individual 3.III.1 displaying profound muscle weakness in her first year of life. She never walked independently and became bedridden and required constant non-invasive ventilation at the age of four years. The proband died of a respiratory infection at 4 years of age. Her father, a US air force pilot, was considered unaffected and had slow nerve conduction velocities. Extensive genome and clinical studies did not reveal any competing causes other than the heterozygous Thr1424Met mutation. This is the most extreme phenotype identified in our cohort, making it conceivable that additional factors might have contributed to the aggressive course and involvement of respiratory muscles.

3. Family 8 had ten affected individuals with a broad intrafamilial variability. Patient 8.III.03 was diagnosed with CMT at the age of 14 years. She developed progressive walking difficulties, using a walker at the current age of 47 years. Her most recent CMTES was 11. Since the age of 20 years, she noticed impaired fine motor skills as well as foot drop. Individuals 8.IV.06 (27 years of age) and 8.IV.04 (11 years of age) had been considered asymptomatic with a CMTES of 0 but showed slowed NCV in electrophysiological studies. Considering their younger age at examination, it is conceivable that they will still develop more pronounced clinical signs and symptoms over their life span. At age 53 years, individual 8.III.04, however, still scored normal at clinical examinations, except for borderline compound motor action potentials of the median and peroneal nerve and slightly increased cross sectional areas of arm nerves on ultrasound, which is considered an extremely mild phenotype, despite carrying the variant.

Overall, a correlation between age and severity could be observed, as is common for CMT disease. However, the correlation is weak ($r^2=0.475$, $p<0.001$) (Figure 2B) and variability between age-matched individuals from the same families exceeds the typical observations in other types of demyelinating CMT (Figure 2B).

Histological findings in nerve biopsy

Patient 5:II:1 (age 21y) and patient 8.III.07 (age 7y) had a clinical radial or sural nerve biopsy available for review (Figure 3A). The histology revealed a severe loss of myelinated large axons. Onion bulb formations were common, indicating chronic de- and remyelinating of axons, consistent with a primary demyelinating process. Occasional clusters of regenerated axons indicate axonal loss and attempted regrowth. No inflammatory infiltration was observed. Acutely degenerating fibers were rarely observed. Electron microscopy (performed on a sural nerve specimen from patient 8.III.07) showed marked increase in collagen between remaining fibers, some loss of unmyelinated fibers, and small onion bulb formations. Segmental demyelination became evident in teased nerve fibers. In a tibial anterior muscle biopsy from patient 8.III.07 obtained at the same age, we observed small and large groups of atrophic fibers and an increased number of subsarcolemmal nuclei. Almost all fibers were type I, pointing towards chronic denervation atrophy.

IP_3R3 expression levels

Charcot-Marie-Tooth disease falls into two types, demyelinating CMT1 and axonal CMT2. The former primarily affects Schwann cells. We therefore investigated IP_3R3 expression in relevant cell types. Western blot analysis of cell lysates from cultured rat Schwannoma cells and iPSC-derived motor neurons demonstrated more abundant protein levels of IP_3R3 in Schwannoma cells compared to motor neurons (Figure 3B). To assess the mechanism of action of the p.Thr1424Met mutation, we examined IP_3R3 protein levels in both patient-derived fibroblasts as well as in transfected HEK293 cells overexpressing plasmids encoding the wild-type and p.Thr1424Met fused to HA or MYC tags. A consistent loss of IP_3R3 protein levels in p.Thr1424Met patient fibroblasts was observed (Figure 3C), as well as both HA-tagged and MYC-tagged p.Thr1424Met protein, when compared to their respective controls (Supplementary figure 1A). We then assessed whether loss in IP_3R3protein levels could be related to mutant-specific RNA-decay, as is known for truncating variants (nonsense-mediated decay). cDNA sequencing demonstrated that the mutant mRNA transcript was present under normal conditions and also after treatment with the nonsense-mediated decay inhibitor cycloheximide

(Supplementary figure 1B). These results suggest a possible mechanism affecting the translation or stability of the protein, leading to lower-steady state levels.

The p.Thr1424Met mutation and its effect on dimerization

IP_3R3 functions as a channel complex, forming homo- and hetero-tetramers with itself and its paralogs, IP_3R1 and IP_3R2. Western blot analysis was performed to determine if the reduction in IP_3R3 protein levels observed in patient fibroblasts, also affected protein levels of IP_3R1 and IP_3R2. However, no difference was observed for IP_3R1 and IP_3R2 protein (Supplementary Figure 1B,C). As the localization of the p.Thr1424Met mutation is near the dimerization sites, the p.Thr1424Met mutant was also assessed for pathogenic effects on IP_3R3 tetrameric complex formation, starting with IP_3R3 homodimerization (Supplementary figure 2A). After co-expressing combinations of p.Thr1424Met and wild-type IP_3R3 with HA and MYC-tags, co-immunoprecipitation followed by Western blot analysis was performed to quantify the strength of the interaction. While we did observe a loss of immunoprecipitated and co-immunoprecipitated proteins transfected with p.Thr1424Met constructs, we cannot attribute this effect to loss of dimerization, as we also observed that p.Thr1424Met protein has a lower overall expression in the over-expression models (Supplementary figure 2B and 1A). Using the same co-overexpression method, but in U2OS cells, we observed that the both p.Thr1424Met mutant and wild-type IP_3R3 co-localize with an enrichment at the perinuclear region, as expected for the ER-membrane localization, without any obvious alterations in localization pattern (Supplementary figure 3A). In summary, the p.Thr1424Met mutation does not interfere with either protein localization or homodimerization, and the pathological mechanism of action remains to be elucidated. It is possible that the mutant might exert a dominant negative effect since it can still interact with the WT thereby sequestering it from proper complex assembly.

Electrophysiology of single IP_3R3 channels

We aimed to assess the function of homotetrameric IP_3R3 channels, thus HEK293T cells devoid of endogenous IP_3R were transiently transfected with cDNAs for the wild-type human IP_3R3 (h-IP_3R3) or with the p.Thr1424Met mutant h-IP_3R3. 48 hr later, the cells were harvested and patch-

clamp electrophysiology of their isolated nuclei was performed as described.[29] With 2 μM free Ca^{2+} and 10 μM IP_3 in the pipette solution, optimal ligand concentrations previously shown to elicit maximal channel activity of the rat IP_3R3 (r-IP_3R3)[30], the channel open probability P_o for h-IP_3R3 was 0.80 ± 0.04 (n=23) (Figure 4), similar to that of the rat.[30] The single-channel conductance was 483 ± 16 pS, also like that of the rat channel. The P_o of r-IP_3R3 depends on both the [IP_3] as well as the cytoplasmic $[Ca^{2+}]_{free}$. Reduction of [IP_3] to 1 μM resulted in a lower channel P_o for h-IP_3R3 (0.12 ± 0.02 (n=14); Figure 4), as expected. The cytoplasmic $[Ca^{2+}]_{free}$ dependence of r-IP_3R3 is biphasic, with low and high $[Ca^{2+}]$ resulting in reduced channel P_o.[30] Elevation of $[Ca^{2+}]$ in the pipette solution to 30 μM reduced channel P_o of h-IP_3R3 (0.07 ± 0.02 (n=11); Figure 4). Thus, the biophysical properties and ligand dependencies of the h-IP_3R3 are highly similar those of r-IP_3R3. Under optimal ligand conditions, the P_o of the p.Thr1424Met mutant h-IP_3R3 was similar to that of the WT channel (0.89 ± 0.04 (n=9); Figure 4). In contrast, the channel P_o remained high in both low [IP_3] (0.74 ± 0.05 (n=10)) as well as high $[Ca^{2+}]$ (0.78 ± 0.03 (n=23) (Figure 4). Thus, the p.Thr1424Met mutation results in a gain-of-function of IP_3R3 channel activity under conditions in which the WT channel activity is normally low.

Tissue-specific expression of ITPR proteins

Next, we wanted to understand the tissue specific consequences of *ITPR3* mutations, as the class of IP_3R protein is ubiquitous, but the expression of the different types of IP_3R proteins occurs in a tissue specific fashion. For instance, mutations in *ITPR1* (IP_3R1), the most highly expressed IP_3R in the cerebellum, cause cerebellar ataxia.[7,8] Transcriptome data from Peng *et. al.* [16] was re-analyzed, which included total RNA from peripheral nerve-derived primary human Schwann cells and skin-derived human fibroblasts. We observed that, at RNA level while all three *ITPRs* were expressed in both Schwann cells and fibroblasts, *ITPR3* is the most highly expressed IP_3R in human Schwann cells, compared to *ITPR2,* which has the highest expression in fibroblasts (Supplementary Figure 3B). The abundance and tissue specificity profile of *ITPR3* in Schwann cells supports *ITPR3* mutations causing a demyelinating CMT, a disorder primarily due to dysfunction of the Schwann cells surrounding the peripheral nerves.

Discussion

Here, we report on the unusually high recurrence of the specific *ITPR3* mutation p.Thr1424Met in nine unrelated families, comprising 33 patients with demyelinating Charcot-Marie-Tooth disease (CMT1). While the common CMT1A duplication event is by far the most common cause for demyelinating CMT, this *ITPR3* p.Thr1424Met mutation represents one of the most frequent single pathogenic alleles for CMT.[31,32] The high recurrence and in-depth phenotyping allowed us to uncover that the severity of neuropathy increases in an age-dependent manner, and that the CMTES differences between age-matched individuals from the same families far exceeds observations in other types of demyelinating CMT. Such high intra-familial differences have been found in *TRPV4*-related axonal neuropathies.[33-35]

In fact, the variability in severity, with some patients displaying no symptoms other than reduced NCVs, has impacted linkage and co-segregation studies when investigating single families. Families 1 (USA) and 8 (Australia) remained unsolved for 30 years, despite extensive independent genetic efforts. However, as in family 5, the *de novo* occurrence of the p.Thr1424Met mutation further supports the genetic evidence for pathogenicity. The clinical variability might have also contributed to misleadingly isolated cases in nuclear families, which together with the clinical symptoms demonstrate significant overlap with CIDP, further complicating the diagnosis and burdening patients with unnecessary immunosuppressant therapy attempts. Patient 6.II.01 was initially diagnosed with chronic CIDP based on an apparent history of sub-acute onset and patchy motor conduction velocities slowing and was treated with intravenous immunoglobulin without obvious response for eight years before the genetic diagnosis was made.

A unique concern is the premature death of one *ITPR3* patient at 5 years of age (Family 3). While it is possible that additional factors played a role, there is a distinct possibility that unusually severe cases of *ITPR3* p.Thr1424Met currently remain undiagnosed due to incorrect clinical conclusions in family members, presumed *de novo* inheritance, and lack of knowledge of this gene and its variable phenotype. The patterns in clinical variability across the nine families in this study are seemingly random and do not appear to support genetic mechanisms such as anticipation. Most individuals with very mild symptoms showed slowed NCV in the intermediate and demyelinating range. However, besides borderline CMAP of the median and peroneal

nerves, patient 8.III.04 did not show any abnormalities of nerve conduction at the age of 53 years. Incomplete penetrance and/or late onset of symptoms, might therefore complicate diagnoses additionally.

We observed significantly reduced IP_3R3 protein levels associated with the p.Thr1424Met mutation in both the overexpression model as well as endogenously expression in patient-derived fibroblasts. We did not observe altered expression of IP_3R1 or IP_3R2, which is different from the reduced IP_3R2 expression reported by Ronkko *et al.* [11]. Terry *et al.* [36] assessed the effect of three IP_3R3 mutations on the IP_3R3-mediated [Ca^{2+}] signaling and demonstrated that the herein reported p.Thr1424Met mutation, when present in homotetrameric complexes, results in elevated basal Ca^{2+}, which they suggested could be a consequence of a leaky channel.[36] By measuring the single-channel properties of wild-type and mutant h-IP_3R3, we here report that the p.Thr1424Met mutant channel remains highly active under conditions in which the wild-type channel has strongly reduced activity. Low-level constitutive Ca^{2+} release from the endoplasmic reticulum through IP_3R is important for maintaining cellular bioenergetics, likely in all cell types [37], as a consequence of the presence of low [IP_3] under basal conditions. The hyper-activity of the p.Thr1424Met mutant channel in the presence of low [IP_3] observed here may, as suggested [36], deplete endoplasmic reticulum Ca^{2+} stores with consequent activation of Ca^{2+} entry across the plasma membrane, resulting in chronic cytoplasmic Ca^{2+} overload. Such a condition is expected to have wide-reaching cellular consequences, including toxicity. Because IP_3R paralogs can hetero-oligomerize, it is possible that the hyper-activity of the homotetrameric mutant IP_3R3 channel observed here could be reduced in heterotetrameric channels incorporating wild-type IP_3Rs. This could be a mechanism that contributes to the variable penetrance of the neuropathy. Future electrophysiological and Ca^{2+} imaging studies are necessary to test this hypothesis. Despite the evidence that the p.Thr1424Met mutation results in a gain-of-function of single-channel activity, the fact that the mutant channel is present at reduced protein levels suggests that an important remaining question is whether neuropathy-associated *ITPR3* mutations act through a loss-of-function or a dominant-negative mechanism of action. Genetically, the frequency of truncating variants and thus the low constraint of pLof=0 in GnomADv4, argue against haploinsufficiency as a mechanism of action. A toxic dominant-negative effect could lead to dysfunction of homo- and heterotrimeric IP_3R channels.

Our study substantiates the genetic evidence for the pathogenic nature of *ITPR3* p.Thr1424Met in demyelinating Charcot-Marie-Tooth disease. The identification of 33 patients with this mutation allowed for a thorough analysis of the remarkable clinical variability of *ITPR3* neuropathy. Additional functional studies will be required to fully establish the mechanism of action and to plan treatment strategies accordingly.

Data availability

The data presented in this study are available from the corresponding author upon request.

Acknowledgements

We are grateful to the families, who were incredibly supportive to this study. We would like to thank the lab of David Yule (University of Rochester) for providing us with IP_3R1 and IP_3R2 antibodies and Elizabeth Jacobs (Saporta lab – University of Miami) for providing us with iPSC-derived motor neurons.

Funding

We thank the patients and their families for study participation. D.B. is supported by a Humboldt Research Fellowship Programme for Postdocs. M.F.D. has received funding by the German Research Foundation (Deutsche Forschungsgemeinschaft, DFG, DO 2386/1-1). J.K.F. is supported by NIH grant R35-GM-140975. S.Z. is supported by the CMT Association, the MDA, CMT-RF, cmt1jfoundation.org, and NIH grants 5U54NS065712 and 5R01NS105755. M.L.K and S.V received funding from the Australian Medical Research Future Fund (MRFF) Genomics Health Futures Mission Grant 2007681. Y.C.L. is supported by Taiwan National Science and Technology Council grants (109-2314-B-075-044-MY3; 112-2314-B-075-034-MY3). MMR is supported by the Medical Research Council (MRC MR/S005021/1), Wellcome Trust (G104817), National Institutes of Neurological Diseases and Stroke and office of Rare Diseases

(U54NS065712 and 1UOINS109403-01), Muscular Dystrophy Association (MDA510281), and Charcot Marie Tooth Association (CMTA).

Competing interests

The authors report no competing interests.

Supplementary material

Supplementary material is available at *Brain* online.

References

1. Berridge MJ. The Inositol Trisphosphate/Calcium Signaling Pathway in Health and Disease. *Physiol Rev*. Oct 2016;96(4):1261-96. doi:10.1152/physrev.00006.2016

2. Wojcikiewicz RJH. The Making and Breaking of Inositol 1,4,5-Trisphosphate Receptor Tetramers. *Messenger (Los Angel)*. Jun 2018;6(1-2):45-49. doi:10.1166/msr.2018.1073

3. Foskett JK, White C, Cheung KH, Mak DO. Inositol trisphosphate receptor Ca2+ release channels. *Physiol Rev*. Apr 2007;87(2):593-658. doi:10.1152/physrev.00035.2006

4. Newton CL, Mignery GA, Sudhof TC. Co-expression in vertebrate tissues and cell lines of multiple inositol 1,4,5-trisphosphate (InsP3) receptors with distinct affinities for InsP3. *J Biol Chem*. Nov 18 1994;269(46):28613-9.

5. Vervloessem T, Yule DI, Bultynck G, Parys JB. The type 2 inositol 1,4,5-trisphosphate receptor, emerging functions for an intriguing Ca(2)(+)-release channel. *Biochim Biophys Acta*. Sep 2015;1853(9):1992-2005. doi:10.1016/j.bbamcr.2014.12.006

6. Ivanova H, Vervliet T, Missiaen L, Parys JB, De Smedt H, Bultynck G. Inositol 1,4,5-trisphosphate receptor-isoform diversity in cell death and survival. *Biochim Biophys Acta*. Oct 2014;1843(10):2164-83. doi:10.1016/j.bbamcr.2014.03.007

7. van de Leemput J, Chandran J, Knight MA, et al. Deletion at ITPR1 underlies ataxia in mice and spinocerebellar ataxia 15 in humans. *PLoS Genet*. Jun 2007;3(6):e108. doi:10.1371/journal.pgen.0030108

8. Synofzik M, Helbig KL, Harmuth F, et al. De novo ITPR1 variants are a recurrent cause of early-onset ataxia, acting via loss of channel function. *Eur J Hum Genet*. Nov 2018;26(11):1623-1634. doi:10.1038/s41431-018-0206-3

9. Toews JC, Schram V, Weerth SH, Mignery GA, Russell JT. Signaling proteins in the axoglial apparatus of sciatic nerve nodes of Ranvier. *Glia*. Jan 15 2007;55(2):202-13. doi:10.1002/glia.20448

10. Schabhuttl M, Wieland T, Senderek J, et al. Whole-exome sequencing in patients with inherited neuropathies: outcome and challenges. *J Neurol*. May 2014;261(5):970-82. doi:10.1007/s00415-014-7289-8

11. Ronkko J, Molchanova S, Revah-Politi A, et al. Dominant mutations in ITPR3 cause Charcot-Marie-Tooth disease. *Ann Clin Transl Neurol*. Oct 2020;7(10):1962-1972. doi:10.1002/acn3.51190

12. Lassuthova P, Safka Brozkova D, Krutova M, et al. Improving diagnosis of inherited peripheral neuropathies through gene panel analysis. *Orphanet J Rare Dis*. Aug 22 2016;11(1):118. doi:10.1186/s13023-016-0500-5

13. Rossor AM, Polke JM, Houlden H, Reilly MM. Clinical implications of genetic advances in Charcot-Marie-Tooth disease. *Nat Rev Neurol*. Oct 2013;9(10):562-71. doi:10.1038/nrneurol.2013.179

14. Gonzalez M, Falk MJ, Gai X, Postrel R, Schule R, Zuchner S. Innovative genomic collaboration using the GENESIS (GEM.app) platform. *Hum Mutat*. Oct 2015;36(10):950-6. doi:10.1002/humu.22836

15. Saporta MA, Dang V, Volfson D, et al. Axonal Charcot-Marie-Tooth disease patient-derived motor neurons demonstrate disease-specific phenotypes including abnormal electrophysiological properties. *Exp Neurol*. Jan 2015;263:190-9. doi:10.1016/j.expneurol.2014.10.005

16. Peng K, Sant D, Andersen N, et al. Magnetic separation of peripheral nerve-resident cells underscores key molecular features of human Schwann cells and fibroblasts: an immunochemical and transcriptomics approach. *Sci Rep*. Oct 28 2020;10(1):18433. doi:10.1038/s41598-020-74128-3

17. Ge SX, Son EW, Yao R. iDEP: an integrated web application for differential expression and pathway analysis of RNA-Seq data. *BMC Bioinformatics*. Dec 19 2018;19(1):534. doi:10.1186/s12859-018-2486-6

18. Beijer D, Deconinck T, De Bleecker JL, et al. Nonsense mutations in alpha-II spectrin in three families with juvenile onset hereditary motor neuropathy. *Brain*. Sep 1 2019;142(9):2605-2616. doi:10.1093/brain/awz216

19. Mak DO, Vais H, Cheung KH, Foskett JK. Patch-clamp electrophysiology of intracellular Ca2+ channels. *Cold Spring Harb Protoc*. Sep 1 2013;2013(9):787-97. doi:10.1101/pdb.top066217

20. Mak DO, McBride S, Foskett JK. ATP regulation of recombinant type 3 inositol 1,4,5-trisphosphate receptor gating. *J Gen Physiol*. May 2001;117(5):447-56. doi:10.1085/jgp.117.5.447

21. Vais H, Foskett JK, Ullah G, Pearson JE, Mak DO. Permeant calcium ion feed-through regulation of single inositol 1,4,5-trisphosphate receptor channel gating. *J Gen Physiol*. Dec 2012;140(6):697-716. doi:10.1085/jgp.201210804

22. Mak DO, Pearson JE, Loong KP, Datta S, Fernandez-Mongil M, Foskett JK. Rapid ligand-regulated gating kinetics of single inositol 1,4,5-trisphosphate receptor Ca2+ release channels. *EMBO Rep*. Nov 2007;8(11):1044-51. doi:10.1038/sj.embor.7401087

23. Qin F, Auerbach A, Sachs F. A direct optimization approach to hidden Markov modeling for single channel kinetics. *Biophys J*. Oct 2000;79(4):1915-27. doi:10.1016/S0006-3495(00)76441-1

24. Bruno WJ, Ullah G, Mak DO, Pearson JE. Automated maximum likelihood separation of signal from baseline in noisy quantal data. *Biophys J*. Jul 2 2013;105(1):68-79. doi:10.1016/j.bpj.2013.02.060

25. Vais H, Siebert AP, Ma Z, Fernandez-Mongil M, Foskett JK, Mak DO. Redox-regulated heterogeneous thresholds for ligand recruitment among InsP3R Ca2+-release channels. *Biophys J*. Jul 21 2010;99(2):407-16. doi:10.1016/j.bpj.2010.04.034

26. Cheng J, Novati G, Pan J, et al. Accurate proteome-wide missense variant effect prediction with AlphaMissense. *Science*. Sep 22 2023;381(6664):eadg7492. doi:10.1126/science.adg7492

27. Danzi M, Dohrn M, Fazal S, et al. Deep structured learning realizes variant prioritization for Mendelian diseases. 2022;doi:10.21203/rs.3.rs-1602211/v1

28. Rentzsch P, Witten D, Cooper GM, Shendure J, Kircher M. CADD: predicting the deleteriousness of variants throughout the human genome. *Nucleic Acids Res*. Jan 8 2019;47(D1):D886-D894. doi:10.1093/nar/gky1016

29. Mak DO, Vais H, Cheung KH, Foskett JK. Nuclear patch-clamp electrophysiology of Ca2+ channels. *Cold Spring Harb Protoc*. Sep 1 2013;2013(9):885-91. doi:10.1101/pdb.prot073064

30. Mak DO, McBride S, Foskett JK. Regulation by Ca2+ and inositol 1,4,5-trisphosphate (InsP3) of single recombinant type 3 InsP3 receptor channels. Ca2+ activation uniquely distinguishes types 1 and 3 insp3 receptors. *J Gen Physiol*. May 2001;117(5):435-46. doi:10.1085/jgp.117.5.435

31. DiVincenzo C, Elzinga CD, Medeiros AC, et al. The allelic spectrum of Charcot-Marie-Tooth disease in over 17,000 individuals with neuropathy. *Mol Genet Genomic Med*. Nov 2014;2(6):522-9. doi:10.1002/mgg3.106

32. Pipis M, Rossor AM, Laura M, Reilly MM. Next-generation sequencing in Charcot-Marie-Tooth disease: opportunities and challenges. *Nat Rev Neurol*. Nov 2019;15(11):644-656. doi:10.1038/s41582-019-0254-5

33. Evangelista T, Bansagi B, Pyle A, et al. Phenotypic variability of TRPV4 related neuropathies. *Neuromuscul Disord*. Jun 2015;25(6):516-21. doi:10.1016/j.nmd.2015.03.007

34. Aharoni S, Harlalka G, Offiah A, Shuper A, Crosby AH, McEntagart M. Striking phenotypic variability in familial TRPV4-axonal neuropathy spectrum disorder. *Am J Med Genet A*. Dec 2011;155A(12):3153-6. doi:10.1002/ajmg.a.34327

35. Fawcett KA, Murphy SM, Polke JM, et al. Comprehensive analysis of the TRPV4 gene in a large series of inherited neuropathies and controls. *J Neurol Neurosurg Psychiatry*. Dec 2012;83(12):1204-9. doi:10.1136/jnnp-2012-303055

36. Terry LE, Arige V, Neumann J, et al. Missense mutations in inositol 1,4,5-trisphosphate receptor type 3 result in leaky Ca(2+) channels and activation of store-operated Ca(2+) entry. *iScience*. Dec 22 2022;25(12):105523. doi:10.1016/j.isci.2022.105523

37. Cardenas C, Miller RA, Smith I, et al. Essential regulation of cell bioenergetics by constitutive InsP3 receptor Ca2+ transfer to mitochondria. *Cell*. Jul 23 2010;142(2):270-83. doi:10.1016/j.cell.2010.06.007

Figure legends

Figure 1 Pedigrees of families carrying the p.Thr1424Met variant. Family pedigrees demonstrating dominant (family 1-4 and 6-9) and *de novo* (family 5) inheritance of the p.Thr1424Met variant in *ITPR3*. Carriers are shown by +/-, non-carriers by -/-. Individuals indicated with # show very mild signs of neuropathy without fulfilling the clinical diagnosis of CMT, hearsay affected individuals are indicated in grey.

Figure 2 Intrafamilial variability of phenotype associated with the p.Thr1424Met *ITPR3* variant. (**A**) demonstrated by clinical pictures of four individuals from family 1. (**B**) plotted by CMTES-2 score vs age (in years); higher score reflects a more severe disease. Individuals from the same family shown in the same color, demonstrating the overall associating between increased age and disease severity (r^2=0.475, p<0.001), meanwhile showing the extreme variability between aged-matched individuals (red box as example). Solid line: linear regression. Dotted line: standard deviation

Figure 3 Nerve biopsy and IP_3R3 expression in Schwannoma, iPSC-derived neurons and p.Thr1424Met patient fibroblasts (**A**) Epoxy section of a radial nerve biopsy of 5:II:1 (age 21y), showing severe loss of myelinated large axons, and most myelinated axons (red asterisks)

are partially surrounded by circumferential cellular processes ("onion bulbs). There is prominent endoneurial collagen (c) and two clusters of regenerated axons are marked by arrowheads, two small axons with "redundant myelin loops" are marked by arrows. Scale bar: 10 microns, (B) comparative protein abundance by immunoblotting of iPSC-derived motor neurons and rat Schwannoma cells probed for $IP_3R3$and loading-control beta-tubulin, (D) immunoblotting of patient-derived fibroblasts of two biological replicate controls and one Thr1424Met *ITPR3* mutation carrier (patient 1) (2 technical replicates each) probed IP3R3 protein, normalized to GAPDH expression, showing reduced IP_3R3. Relative expression differences were determined across three replicate blots from separate lysates by one-way ANOVA, ns = not significant, *= $p<0.05$, *** = $p<0.001$.

Figure 4 p.Thr1424Met mutation in human IP_3R3 augments the channel activity under non-optimal ligand conditions. (**A)** Representative traces (2s long) of continuous single-channel recordings at V_m = -30 mV, for wild-type and p.Thr1424Met h-IP_3R3 channels. Ligand conditions ($[IP_3]$ and free $[Ca^{2+}]_{free}$) indicated. Arrows a indicate the channel closed state, (**B**) P_o values for the wild-type and p.Thr1424Met mutant channels in various ligand conditions (indicated on abscissa).

Table 1 Clinical characteristics of the 33 individuals carrying the *ITPR3* p.Thr1424Met mutation in the study

	Clinical characteristics
Total number of individuals (with p.Thr1424Met mutation)	33
Families	9
Mean age at examination, years (youngest–oldest)	44.2 years (11 years–86 years)
Mean age at first walking difficulties, years (youngest–oldest)	20.5 years (1–63 years)
Sex distribution, male:female	15:18
Muscle atrophy	
UL	12/23 (52%)
Upper legs	(31%)
Lower legs	(94%)
Impaired hand function[a]	18/28 (64%)
Walking difficulties	18/28 (64%)
Use of walking aids	
AFO	12/28 (43%)
Walking cane/walker	8/28 (29%)
Wheelchair	6/29 (21%)
Deep tendon reflexes UL	
Normal	10/24 (42%)
Reduced	7/24 (29%)
Absent	7/24 (29%)
Deep tendon reflexes LL	
Normal	1/24 (4%)
Reduced	4/24 (17%)
Absent	19/24 (79%)
Sensory loss (light touch, pallesthesia, and/or pinprick)	
UL	9/24 (38%)
LL	17/24 (71%)
Mean distal ulnar CMAP (mV)	4.6 (0.3-10.3)
Mean distal ulnar mNCV (m/s)	32.5 (20.2-50.7)
Sensory gain	
Paresthesia	12/27 (44%)
Neuropathic pain	7/25 (28%)
Mean CMTES score (lowest–highest)	10 (0–25)

For more detailed individual descriptions of muscle atrophy patterns, muscle strength, and sensory loss, please see supplementary table 1.AFO, ankle-foot orthoses; CMAP, compound motor action potential; CMTES-2, Charcot-Marie-Tooth disease examination score version 2; LL, lower limbs; mNCV, motor nerve conduction velocity; UL, upper limbs.

[a]Assessing difficulties with buttons or cutting food by patient history, according to the CMTES-2.

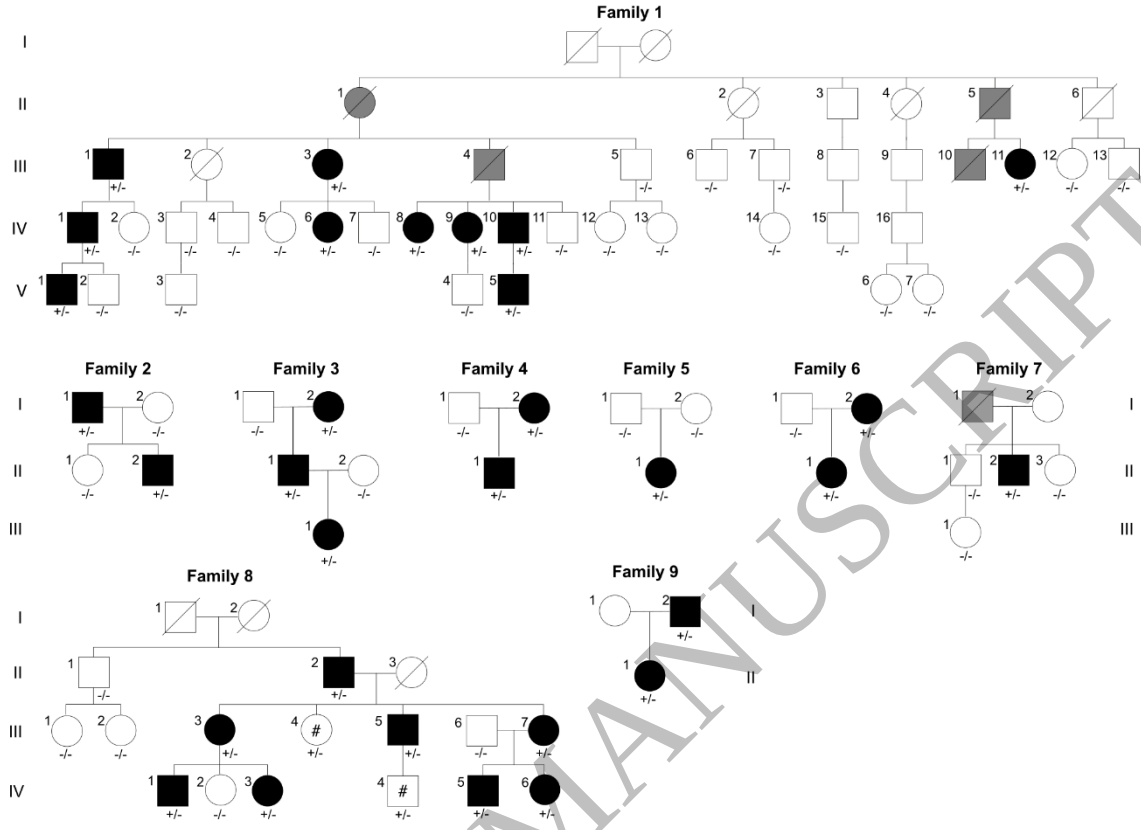

Figure 1
159x115 mm (x DPI)

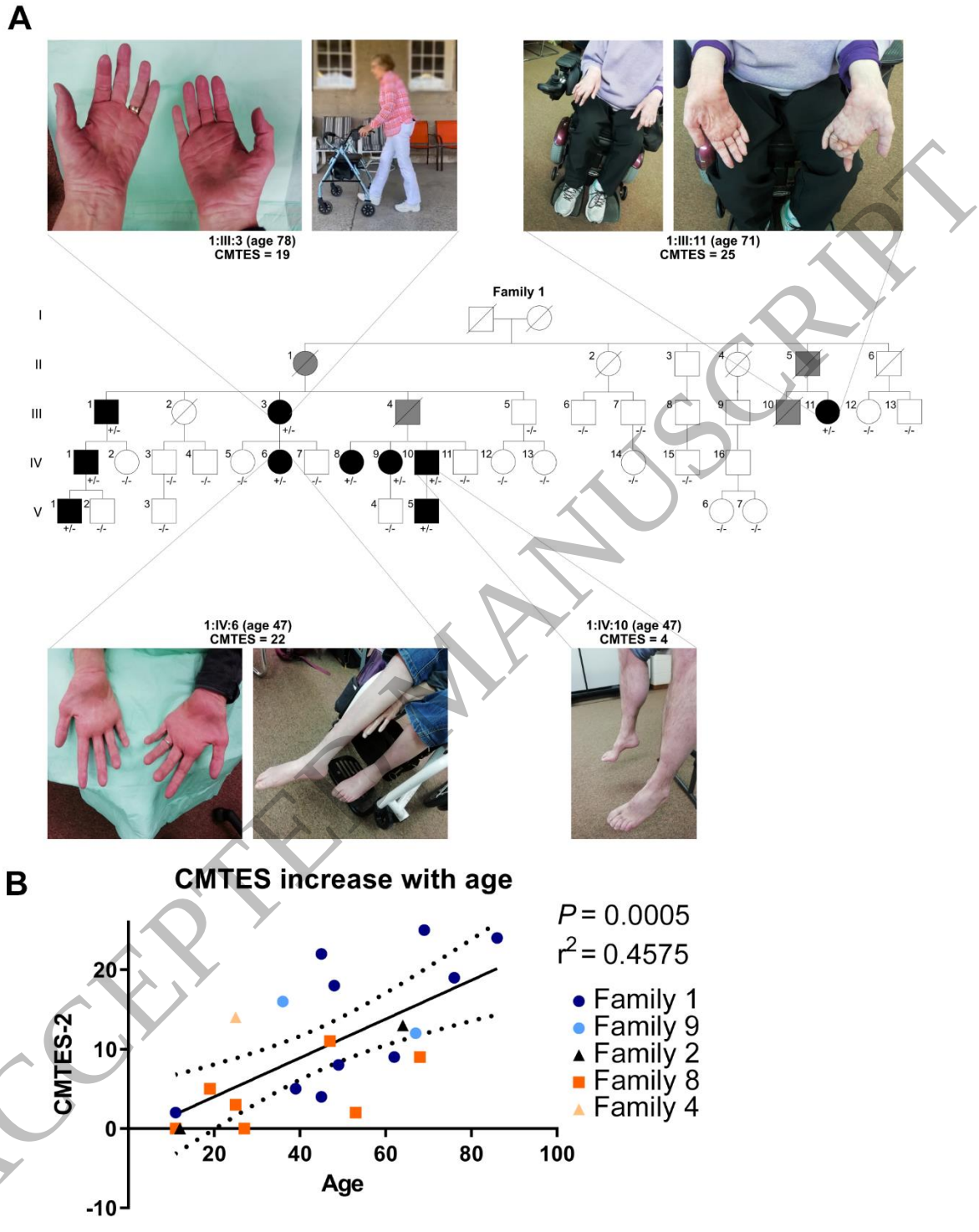

Figure 2
159x197 mm (x DPI)

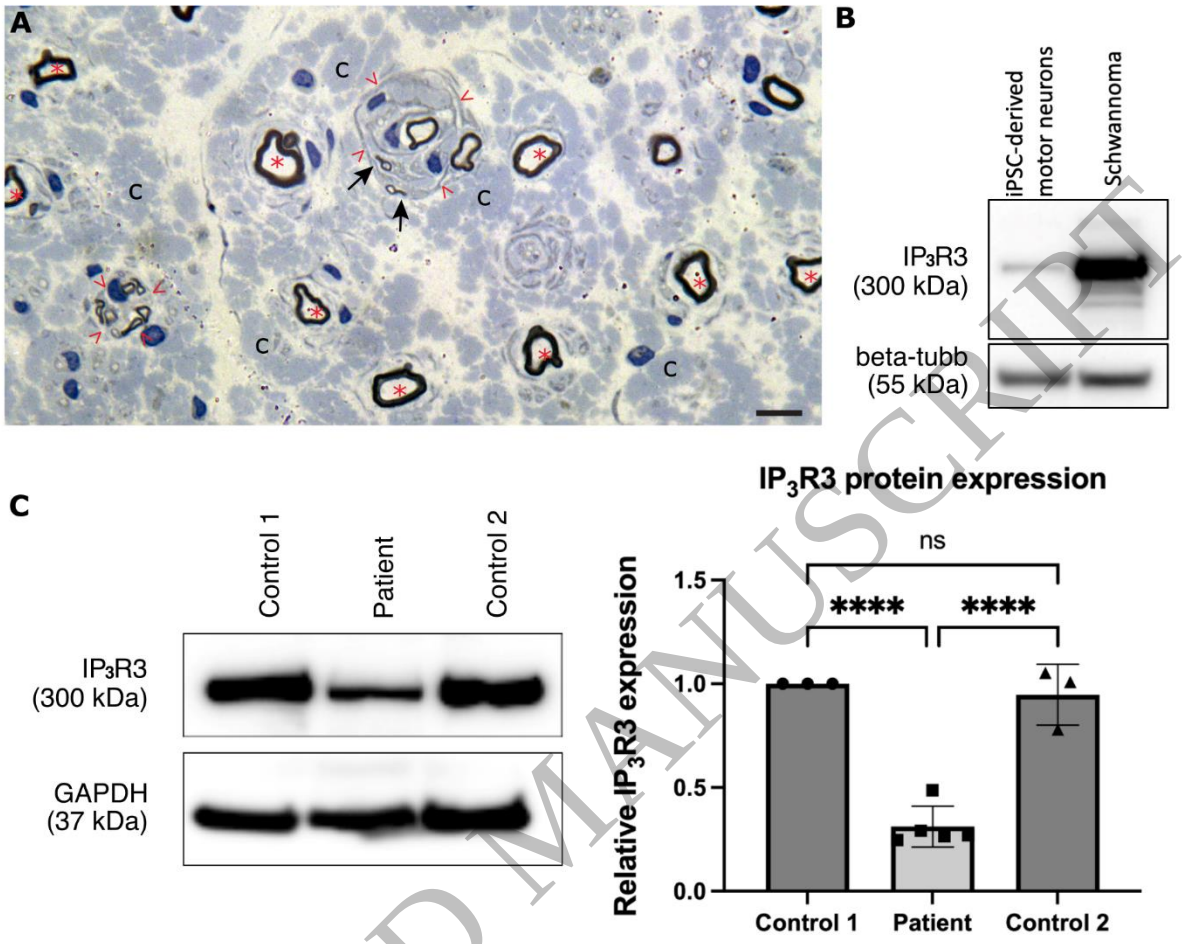

Figure 3
159x126 mm (x DPI)

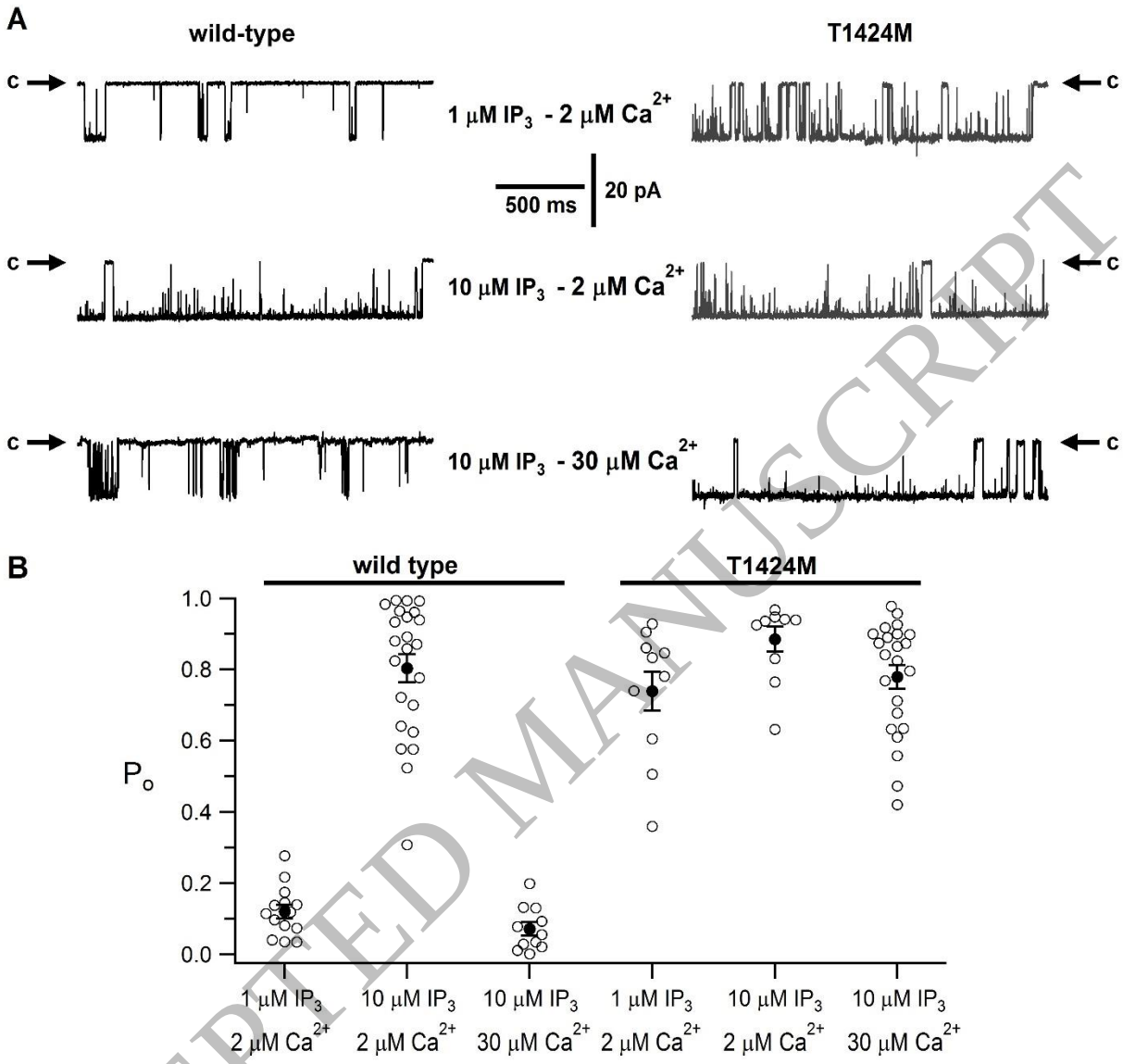

Figure 4
82x54 mm (x DPI)